# Biodegradable, Breathable Leaf Vein-Based Tactile Sensors with Tunable Sensitivity and Sensing Range

*Yue Liu, Juan Tao, Wenkai Yang, Yufei Zhang, Jing Li, Huilin Xie, Rongrong Bao,\* Wenchao Gao,\* and Caofeng Pan\**

Resistive pressure sensors have been widely studied for application in flexible wearable devices due to their outstanding pressure-sensitive characteristics. In addition to the outstanding electrical performance, environmental friendliness, breathability, and wearable comfortability also deserve more attention. Here, a biodegradable, breathable multilayer pressure sensor based piezoresistive effect is presented. This pressure sensor is designed with all biodegradable materials, which show excellent biodegradability and breathability with a three-dimensional porous hierarchical structure. Moreover, due to the multilayer structure, the contact area of the pressure sensitive layers is greatly increased and the loading pressure can be distributed to each layer, so the pressure sensor shows excellent pressure-sensitive characteristics over a wide pressure sensing range (0.03–11.60 kPa) with a high sensitivity (6.33 kPa$^{-1}$). Furthermore, the sensor is used as a human health monitoring equipment to monitor the human physiological signals and main joint movements, as well as be developed to detect different levels of pressure and further integrated into arrays for pressure imaging and a flexible musical keyboard. Considering the simple manufacturing process, the low cost, and the excellent performance, leaf vein-based pressure sensors provide a good concept for environmentally friendly wearable devices.

## 1. Introduction

Human skin, as the largest organ of body, is not only the first protection barrier from the outside world, but also has numerous tactile receptors for perceiving external stimulus, such as pressure, strain, temperature, and humidity.[1–3] Considerable researches have been conducted to develop bioinspired e-skins by mimicking perceiving capability and features of

natural skin, which has significant applications in wearable health care devices, intelligent robotics, implantable medical devices, and human-machine interfaces.[4–7] Different sensing mechanisms including capacitance,[8] piezoresistivity,[9] piezoelectricity,[10] and triboelectricity,[11] have mainly been used to convert external stimuli into electronic impulses for quantitative and spatial detection. Among them, piezoresistive effect has been widely used in the design and fabrication of tactile sensor due to the advantages of large detection, simple signal processing, and strong anti-interference capability.[12–19] Novel materials and structure have been applied in the design of high performance tactile sensors in recent researches. A hybrid 3D structure based on ultralight and superelastic MXene/reduced graphene oxide aerogel is adopted to design a piezoresistive sensor by Yihua Gao etc., which exhibits the sensitivity of 22.56 kPa$^{-1}$, and limit detection (10 Pa).[20] Kai Pan's group reported a piezoresisitive pressure sensor based on aPANF/GA aerogel with a 3D interconnected hierarchical microstructure to monitor the real time movement of wrist pulse and main joints of human body.[21] Tactile sensors with high performance containing high sensitivity, wide detection range, fast response, flexibility, and mechanical durability are most concerned in the recent progress of e-skin.[22] Additionally, special functional properties such as self-healing, self-powered, biodegradable, biocompatible, and

Y. Liu, W. Yang, Y. Zhang, J. Li, R. Bao, W. Gao, C. Pan
CAS Center for Excellence in Nanoscience
Beijing Key Laboratory of Micro-Nano Energy and Sensor
Beijing Institute of Nanoenergy and Nanosystems
Chinese Academy of Sciences
Beijing 101400, P. R. China
E-mail: baorongrong@binn.cas.cn; wenchao.gao1@monash.edu; cfpan@binn.cas.cn
J. Tao, C. Pan
College of Physics and Optoelectronic Engineering
Shenzhen University
Shenzhen 518060, P. R. China

The ORCID identification number(s) for the author(s) of this article can be found under https://doi.org/10.1002/smll.202106906.

H. Xie
Sinoma Synthetic Crystals Co
Ltd
Beijing 100018, P. R. China
R. Bao, C. Pan
Center on Nanoenergy Research
School of Physical Science and Technology
Guangxi University
Nanning, Guangxi 530004, P. R. China
W. Gao
Department of Civil Engineering
Monash University
Clayton 3800, Australia

ADVANCED
SCIENCE NEWS
www.advancedsciencenews.com

NANO · MICRO
small
www.small-journal.com

breathable characteristics have been gradually integrated to obtain a comprehensive performance of e-skin to accommodate the practical applications.[23–28] Especially, breathability is an essential approach to enhance the comfortability of wearable devices by balancing thermal-moisture between the human body and external environment. Bio-degradability allows the implanted devices degraded and resorbed in the body without any harm, so no subsequent operation will be required to remove them when used in medical therapy. Therefore, tactile sensors endowed with breathability and biodegradability are intensively demanded in the applications in wearable health monitoring, biomedical surveillance, and implantable devices, providing great practical significance.

Herein, an all-nanofiber-based biodegradable and breathable pressure sensor on the basis of natural leaf vein is proposed. First of all, the inherent fractal structure of natural leaf vein and 3D porous hierarchical structure of the device enable the sensor a high sensitivity of 6.33 kPa$^{-1}$ over a wide sensing range of pressure (0.03–11.6 kPa), which fully meets the requirements of its application as human health monitoring equipment. Moreover, pressure-sensitive characteristics of the sensor can be adjusted by controlling the number of layers so as to accommodate different application scenarios. Furthermore, the pressure sensor is completely composed of biodegradable natural leaf vein, poly(lactic-co-glycolic acid) (PLGA), and polyvinyl alcohol (PVA) nanofiber (NF) film, allowing the device biodegradability. Simultaneously, the NF film and porous structure of leaf vein enables the breathability of the sensors. Then, leaf vein-based sensors are applied onto the human body to monitor physiological signals and joint movements, including vocal cord vibration, pulse, elbow movement, finger bending, and knee movement. Finally, an array of leaf vein-based sensor with breathability and biodegradability is fabricated to obtain pressure mapping and a virtual and flexible musical keyboard for human-machine interface applications.

## 2. Result and Discussion

### 2.1. Structure Design and Sensing Principle of the Multilayer Pressure Sensor

As shown in **Figure 1**a, natural leaf veins of magnolia leaves coated by Ag nanowires (Ag NWs) are adopted as pressure-sensitive materials to fabricate the pressure sensors. After specific treatment and design integration of the leaf vein, a wearable flexible pressure sensor endowed with excellent biocompatibility, environmental friendliness, and breathability are realized. This flexible sensor can be directly attached to the human body for monitoring various signals without any harm, with the multilayer structure shown in Figure 1b. The upper and the lower PLGA NF film is used as encapsulating layer and substrate; the conductive leaf veins coated with Ag NWs and pure natural leaf veins are interlaced and stacked as the pressure-sensitive layers; the upper and lower electrode layers are composed of PVA NF film coated with Ag NWs.

Among them, PLGA and PVA NF films are prepared by electrospinning method. Natural leaf vein is obtained from mature magnolia leaves and then treated by alkaline hydrolysis method.[29] The preparation method and process of specific materials and devices are illustrated in Figure S1 (Supporting Information). Figure 1c shows the three-dimensional porous hierarchical structure of the pressure-sensitive layer, which is composed of multiple leaf veins and the distribution of Ag NWs on them.

The leaf vein-based pressure-sensitive layers greatly increase the contact area between layers by using multilayer geometry, which is an effective method to achieve high sensitivity over a large sensing range.[30]

In addition, in order to obtain uniform films, different conditions of electrospinning are tried. The solution concentrations of PLGA are 6.5, 7.5, 8.5, and 9.5 wt%, and the solution concentrations of PVA are 9, 10, and 11 wt%, respectively. The scanning electron microscope (SEM) images of the PLGA and PVA NF films with different polymer solution concentrations are shown in Figure S3 (Supporting Information). When the polymer concentration is low, the polymer chain will break before it reaches the collector, forming beaded or string NFs. With the increase of the concentration of the polymer solution, the uniform beadless NFs can be realized due to an increase in the viscosity of the solution. Once the concentration of the solution exceeds a certain value, the flow of the solution will be blocked, resulting in defective or beaded NFs. Hence, uniform NF films without beads can be prepared when the concentration of PLGA and PVA are 8.5 and 10 wt%, respectively. Moreover, the contact angles of PLGA and PVA NF films are also tested. As displayed in Figure S4 (Supporting Information), the contact angle of PLGA NF film is about 124.6°, demonstrating an excellent hydrophobicity. On the other hand, PVA NF film presents the hydrophilicity with the contact angle of 62.5°. The pressure sensor is conducive to the heat dissipation and perspiration of the human body.

The fundamental working principle of the leaf vein-based pressure sensor is piezoresistive effect. When the external pressure is applied onto the surface of the sensor, the distance between the conductive layers and the electrodes will decrease, which leads to the reduction of the total resistance of the leaf vein-based pressure sensor because of the formation of more conductive pathways.[31] Therefore, the output current is gradually enhanced with the increase of the pressure, as shown in the Figure 1d. Moreover, the pressure sensor is composed of conductive Ag NWs-coated leaf vein layer and natural leaf vein isolation layer, so the initial current of the device is very small without external load, which can effectively reduce the power consumption to a large extent.

### 2.2. Electrical Output Performance

As a pressure sensor to monitor the physiological signals and the movement of mainly joints of human body, it is required to have a relatively high performance of sensors.[32–34]

In order to optimize the sensitivity and linear sensing range of the leaf vein-based pressure sensor, different Ag NWs contents mixed into the pressure-sensitive layer have been discussed. The illustration in **Figure 2**a shows the SEM images of Ag NWs with different contents being wound on the leaf vein, which proves that Ag NWs have been successfully introduced into the pressure-sensitive layers. As shown in Figure 2a, the
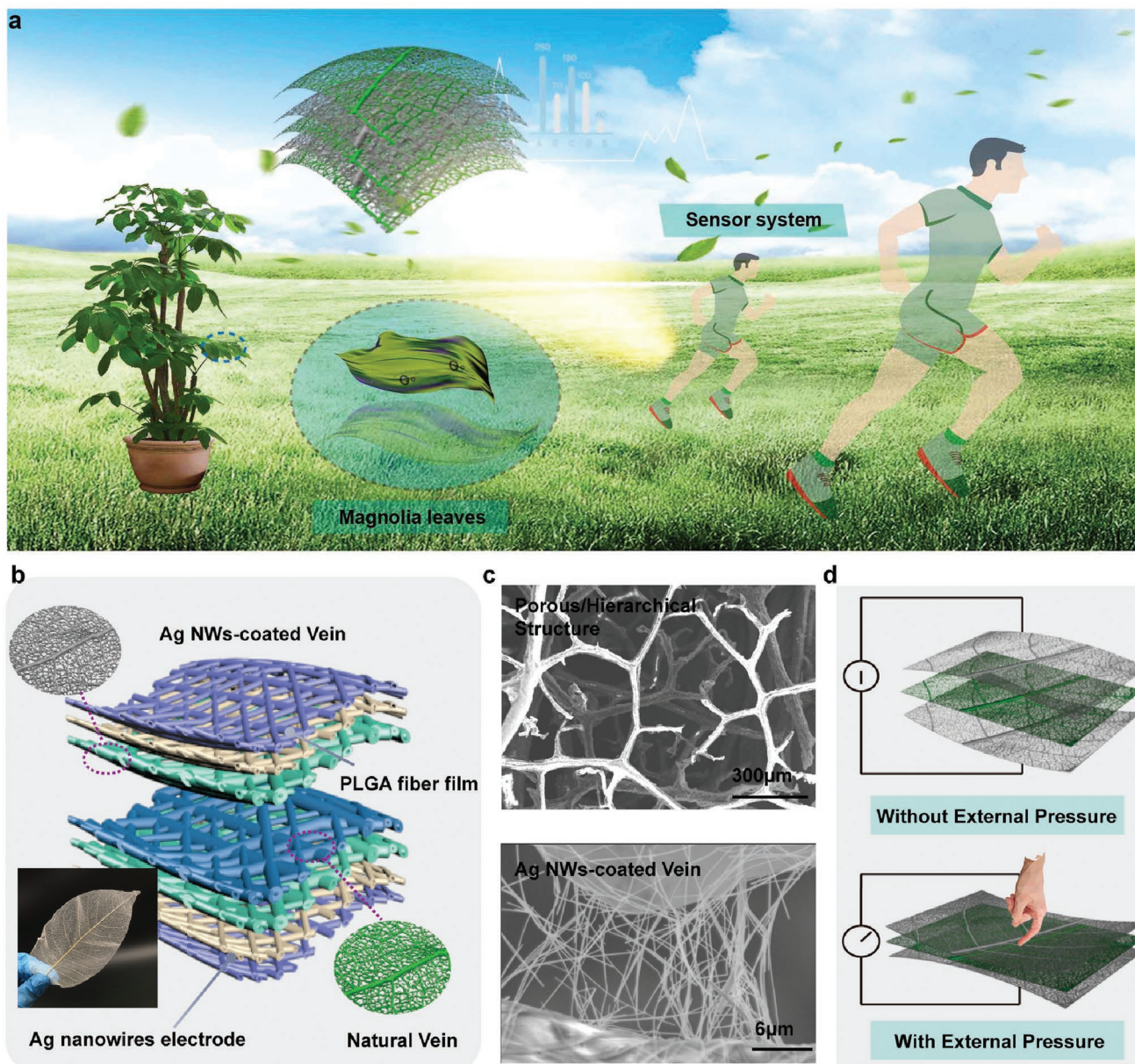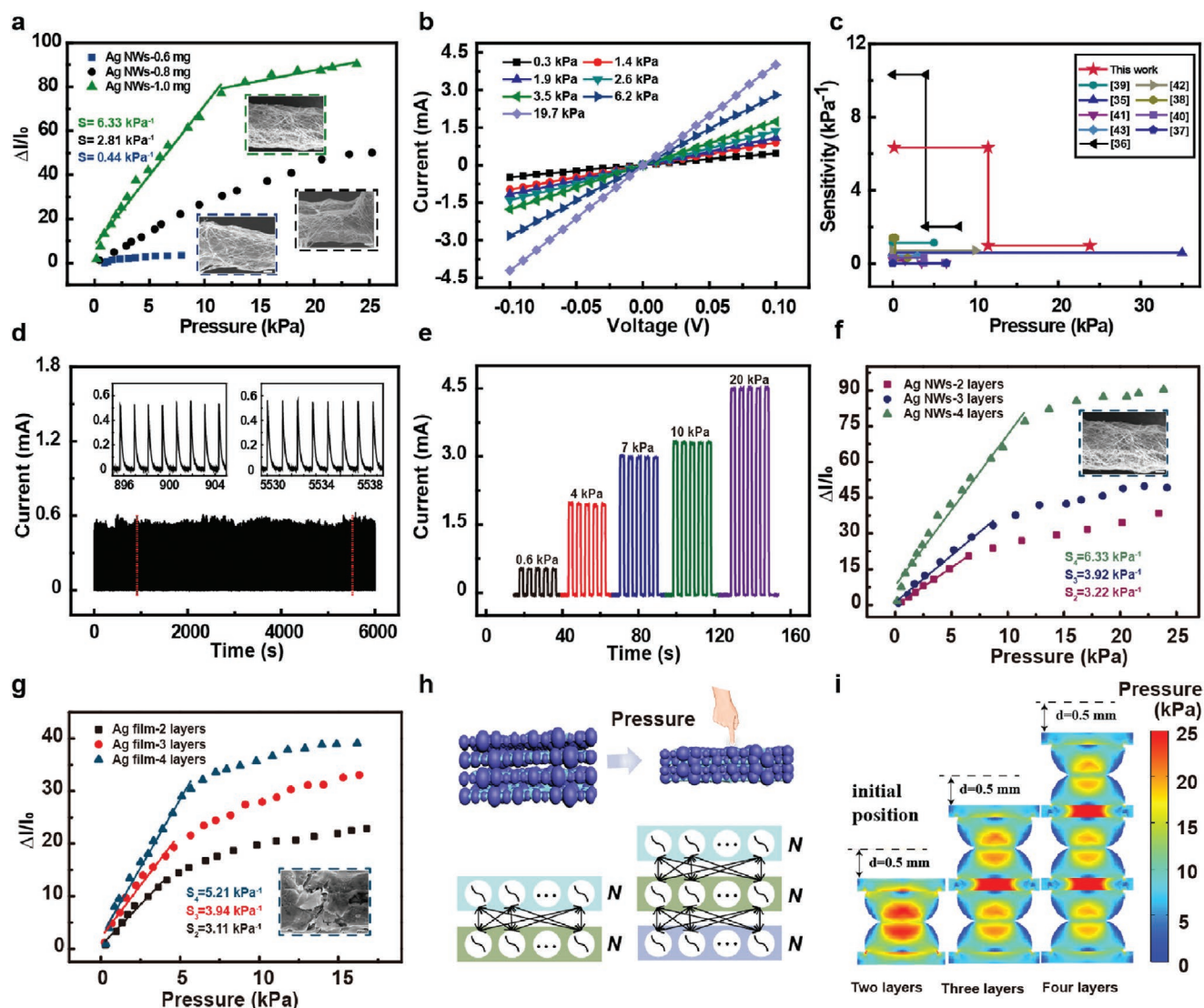
**Figure 1.** a) Leaf vein-based pressure sensor system for human health monitoring and joint movement detection. The materials of pressure-sensitive layers are Magnolia leaf veins from nature. They can be integrated with electrical system and used as the environmentally friendly flexible pressure sensors. b) Multilayer structure of the leaf vein-based pressure sensor. c) SEM images of surface morphology of the leaf vein-based pressure sensitive layer including 3D porous hierarchical structure (top) and the Ag NWs wound around the leaf veins (bottom) (scale bars, 300 μm and 6 μm). d) Sensing principle of the device based on piezoresistivity.

sensitivity of the leaf vein-based pressure sensor is significantly improved with the increase of the content of Ag NWs, and the linear sensing range is also increased in a consistent trend. When the content of Ag NWs is increased to 1.0 mg, the sensitivity is improved to 6.33 kPa$^{-1}$, which is about 14 times higher than that of 0.6 mg. Meanwhile, compared with the content of Ag NWs of 0.6 mg, the linear detection range is also enhanced to 11.60 kPa. Additionally, the current–voltage curves of the pressure sensor with four conductive leaf vein layers are tested under different external loading pressures, as shown in Figure 2b. The pressure is increased from 0.3 to

19.7 kPa, and the leaf vein-based pressure sensor shows good ohmic contact.

Figure 2c is a comparison of the pressure sensing performance of our leaf vein-based multilayer pressure sensor with other devices in other some literatures.[35–45] Some pressure sensors have a large sensing rang but in a low sensitivity. Although some others' sensitivity is high, the detection range is narrow and nonlinear.[46–51] The leaf vein-based pressure sensor in this work has a relatively high sensitivity over a wide linear detection range, offering great superiority as the wearable electronics for the whole human body. Specific comparison of more

**ADVANCED
SCIENCE NEWS**

www.advancedsciencenews.com

NANO · MICRO

**small**

www.small-journal.com

**Figure 2.** Electrical output performance of the leaf vein-based pressure sensor with four pressure sensitive layers. a) Responses of current to different external pressures of devices with different content of Ag NWs at 0.1 V. The inset SEM images are the leaf vein with different content Ag NWs (scale bars, 6 μm). b) I–V curves of the device under different external pressure. c) Comparison of performance between our leaf vein-based pressure sensor and some homogeneous pressure sensors. d) Repeatability and reproducibility of the device under the pressure of 500 Pa at 0.1 V. e) Dynamic responses of the device to different external pressures under loading-unloading cycles. f) Sensitivity response curves comparison of the devices between different pressure sensitive layers (two, three, and four) when the conductive filler is Ag NWs. The inset SEM images is the leaf vein covered by Ag NWs (scale bars, 6 μm). g) Sensitivity response curves comparison of the devices between different pressure sensitive layers (two, three, and four) when the conductive filler is Ag film. The inset SEM image is the leaf vein covered by Ag film (scale bars, 3 μm). h) Model of conductive channels formed by multilayer devices under external pressure. i) Simulation schematic diagram of the contact area and pressure distribution of different pressure-sensitive layer by COMSOL.

performances between those pressure sensors in literatures is listed in Table S1 (Supporting Information). Simultaneously, repeatability and reproducibility of the pressure sensor are also important performance evaluations when considered in the practical applications. As displayed in Figure 2d, the response curves remain nearly constant after 6000 loading cycles under applied pressure of 500 Pa, indicating an excellent repeatability and reproducibility of the leaf vein-based pressure sensor. As for the response time, the device exhibits an increasing response time and relaxation time about 161 and 227 ms, respectively, seen in Figure S5 (Supporting Information).

The dynamic response of the leaf vein-based pressure sensor under the loading-unloading pressure cycle is shown in Figure 2e. The device displays a stable instantaneous response within the pressure range of 0.6 to 20 kPa, verifying a valid response to different external pressures. Furthermore, the detection limit of the pressure as low as 30 Pa has been demonstrated on the basis of vein-based pressure sensor (Figure S6, Supporting Information). Since the normal blood pressure of human body fluctuates within the range of 2.7 to 4 kPa, our leaf vein-based pressure sensor can be used as an available approach to monitoring physiological signals of human body sufficiently.

In addition to the optimization and characterization of the basic pressure sensing performance of the leaf vein-based pressure sensor described above, the influence of the multilayer structure on the electrical output performance of the device is further discussed. In Figure 2f,g, Ag NWs and Ag film are used as conductive fillers to design following experiments, indicating that the conductive leaf veins with different layers as the pressure sensing layer have a certain effect on the electrical output performance of the devices. When the conductive leaf veins in pressure sensitive layers is two layers, the sensitivity and linear detection range of the device is 3.22 kPa$^{-1}$ and 6.5 kPa. When the conductive leaf veins increase to four layers, the sensitivity and linear detection range of the device have been both improved to 6.33 kPa$^{-1}$ and 11.6 kPa. In order to further explain the influence of hierarchical structure on the sensitivity and linear detection range of devices in detail. Firstly, as shown in Figure 2h, when the device is loaded with external pressure, the layer spacing between conductive layers will gradually reduce to form more conductive channels. For the hierarchical structure, it is assumed that each layer of conductive leaf vein has the number of N contact protruded points as the conductive points. When two layers are closely stacked together, the number of conductive channels of $N^2$ can be formed. Similarly, the number of conductive channels of $N^3$ and $N^4$ will be obtained when three and four layers are closely stacked together, respectively. As long as the number of conductive leaf vein layers is increased by one layer, the number of conductive channels is increased by $N$ times. The increase in the number of conductive channels makes the sensitivity and linear detection range of the device improved.[30] Furthermore, according to the distribution of external pressure inside the multilayer pressure sensors simulated by COMSOL in Figure 2i and Figure S8 (Supporting Information), it can be found that the increase of the number of pressure-sensitive layers will result in a larger contact area between layers and a less distribution of same external pressure in each layer, yielding a high sensitivity response within a wide linear detection range of the device.[30] Besides, we also use the simplified model of superimposed hierarchical conductive leaf vein to theoretically calculate and analyze the total resistance of the pressure sensor, with detailed calculation section described in Figure S9 (Supporting Information).[52] It can be observed that the sensitivity of the pressure sensor can be improved by the increase of the number of conductive leaf veins. Considering the comfortable feeling and high performance when used in wearable applications, the pressure sensing layers are designed as four layers instead of a thicker choice. Therefore, the electrical output performance of the device can be tuned by changing the number of pressure sensing layers, providing another approach for the design of adjustable performance devices in different application scenarios.

## 2.3. Breathability and Biodegradability

Wearable tactile sensor with breathable and waterproof property has significant effect in modern social life, which is a goal that people have been striving for.[53–58] As exhibited in **Figure 3**a, pressure sensor based on leaf veins and NF films can be directly attached to the skin. Benefiting by its hierarchical porous structure, when attached to the human skin, the sweat from the human body can be quickly dissipated through the pressure sensor to the surrounding environment. At the same time, due to the hydrophobicity of the PLGA packaging layer, the pressure sensor is endowed with a certain waterproof ability. Moreover, in order to design a pressure sensor with better biocompatibility and more suitable for people to wear for a long time, it is vital in the choice of fabricated materials. PLGA and PVA NF films are selected as the materials for the packaging layers, substrate and electrode, respectively. PLGA is a biodegradable functional polymer organic compound. Its degradation products are lactic acid and glycolic acid, which are also by-products of human metabolic pathway. Therefore, PLGA has good biocompatibility without toxic side effects in application.[59,60] PVA is also environmentally friendly organic polymer with the dual characteristics of water solubility and biodegradation, and can be completely degraded into carbon dioxide ($CO_2$) and water ($H_2O$).[61] The Fourier transform infrared spectrum (FTIR) of PLGA and PVA NF films show that the chemical composition and structural characteristics of the materials still remain constant after electrospinning (Figure S11, Supporting Information).[62–64] What's more, as the conductive fillers, Ag NWs also have a certain antibacterial function.[65,66] Moreover, nature leaf veins with microstructure are adopted to design the sensor, with surface morphology and SEM image illustrated in Figure 3b. It can be seen that the leaf veins have a large number of fracture structure ranging from nanoscale to macroscopic scale (Figure S10, Supporting Information), which has the advantage of optimizing its surface coverage while maintaining air permeability.[67–73] The characteristics of these materials show great advantages in the design and construction of medical equipment for physiological signal monitoring.

The photograph of the natural leaf vein placed on the leaves is shown in Figure 3c. Almost no deformation of the leaves has been seen, which demonstrate its extreme lightness and softness. The whole surface of the natural leaf vein presents a web-like structure like the spider web, which undeniably guarantees the air permeability of the pressure sensor. In order to demonstrate the breathability of the complete packaged device the speed of water vapor molecules penetrating the film is used to evaluate the breathability performance of the leaf vein-based pressure sensor and every functional layer of each part of the device, with optical photographs of process illustrated in Figure 3d.[74] The glass bottles containing water are sealed by whole device, as well as the various functional thin films of devices, including PVA NF film, PLGA NF film, natural leaf veins, and completely airtight parafilm. Afterwards, they are compared with the open glass bottles of the same mass of water that are simultaneously held at room temperature. After 16 days, the water sealed by the whole device, PVA NF film and PLGA NF film are completely evaporated with the intact films, which is the same as the control group with full opening. Inversely, the mass of water in the glass bottle sealed by parafilm almost remains unchanged. During the whole experiment, the weight loss of water is recorded every 24 h (Figure 3e) and the photographs of the process of the weight loss of water are shown in Figure S12 (Supporting Information). According to these results, the device shows excellent breathability.
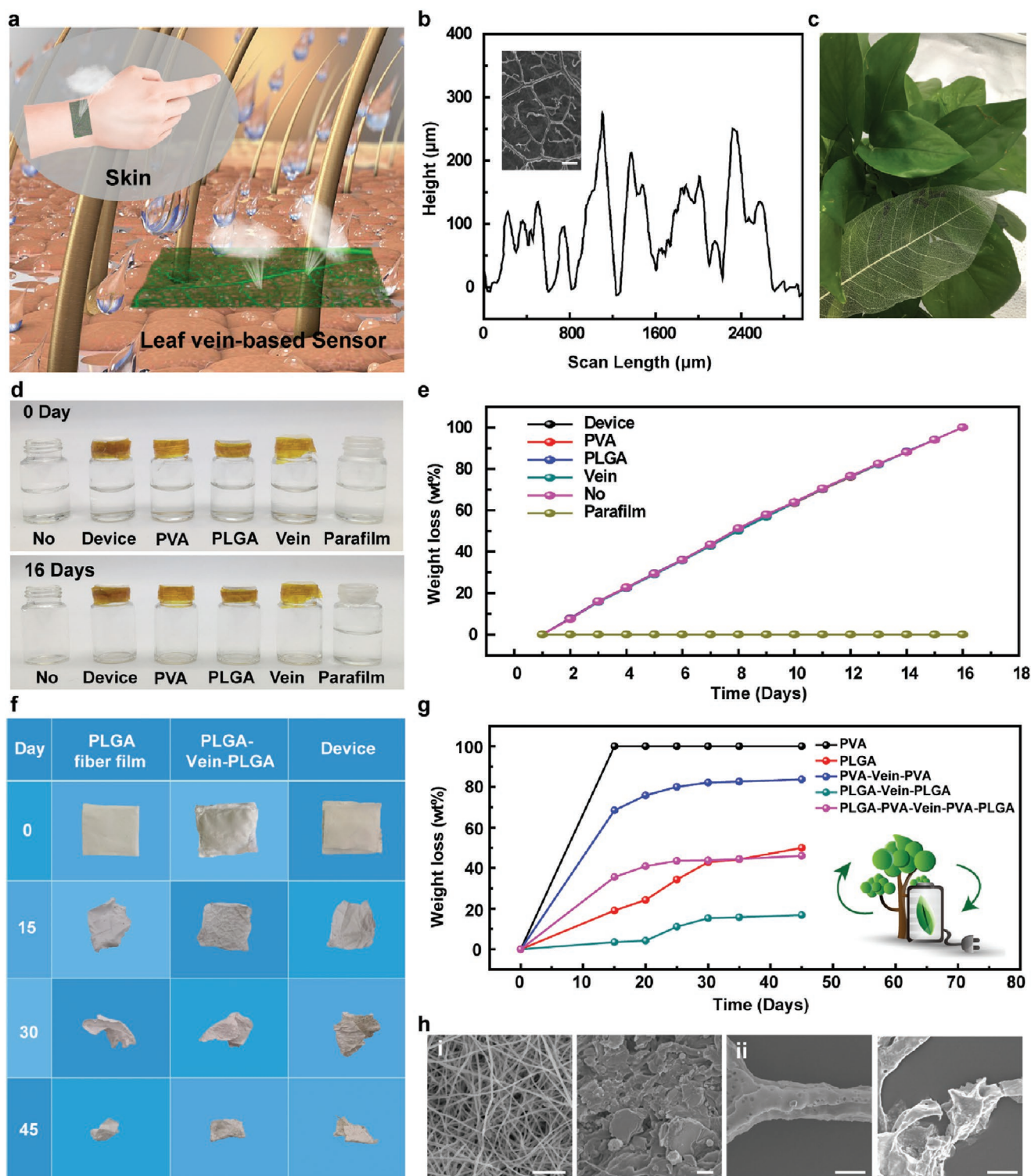
**Figure 3.** Breathability and biodegradability of the leaf vein-based pressure sensor. a) Schematic diagram showing that the leaf vein-based pressure sensor can be directly attached to human skin and has the abilities of watertightness and breathability simultaneously. b) The thickness and surface roughness of the leaf vein. The inset is the SEM image of leaf vein (scale bars, 300 µm). c) Optical photograph of the natural leaf vein. d) Optical photographs of the breathability test process at room temperature. e) Weight loss of water in the glass bottle covered with different NF films per 24 h. f) Photographs of biodegradation process of different NF films, including PLGA, PLGA/Vein/PLGA, and the whole device. g) Weight loss of different NF films during the biodegradation process. h) i. The SEM images of PLGA NF film before (left) and after (right) the 45-day degradation (scale bars, 15 and 3 µm, separately) ii. The SEM images of leaf vein before (left) and after (right) the 45-day degradation (scale bars, 15 µm).

**ADVANCED
SCIENCE NEWS**
www.advancedsciencenews.com

**NANO · MICRO
small**
www.small-journal.com

At the same time, we also carry out the degradability in vitro of the whole device and the films of each functional layer has been carried out for 45 days, including PLGA NF film, PVA NF film, PLGA NF film/leaf vein/PLGA NF film, PVA NF film/leaf vein/PVA NF film, PLGA NF film/PVA NF film/leaf vein/PVA NF film/PLGA NF film. Figure 3f and Figure S13 (Supporting Information) show photographs of whole device and the different functional layers of the device in the degradation process. Due to the rapid autocatalytic hydrolysis and volume degradation of the PVA NF film once it encounters water, the weight loss rate reaches almost 100%, hence the corresponding results cannot be recorded in the Figure 3f. As shown in Figure 3g, the weightlessness of PVA NF film is highly similar to that of PVA NF film/leaf vein/PVA NF film, which further indicates the rapid hydrolysis capacity of PVA NF film. In contrast to PVA NF film, PLGA NF film has stronger resistance to weightlessness and water absorbing initially, but it is slightly contracted and crimped due to the water decomposition of the main chain of the polymer. About 20 days later, the degradation process of PLGA NF film is gradually accelerated. As depicted in Figure 3h (i), some cracks appear on the surface of PLGA NF film at the later stage of degradation when compared with pure PLGA NF film without any treatment. The weight loss of the whole device is 50%. It's worth noting that although the degradation of leaf veins presents a relatively slow rate in the whole process, the structure of leaf veins is also changed with fragmentation and cracks on the surface (Figure 3h (ii)). Moreover, a better degradation effect for leaf veins will be realized by adding the compound cellulolytic enzymes.

### 2.4. Human Health Monitoring and Pressure Sensing Array

Most people in a state of fatigue are suffering from mental stress and sub-health nowadays, and 87.7% of sudden deaths in China occur outside hospitals.[75,76] Therefore, it is of great significance to monitor human physiological signals and movement conditions anytime in contemporary medical treatment and research.[77–79] The pressure sensor based on leaf vein in this work has shown excellent performance according to above results. Therefore, some physiological signals and the movements of major joints, including vocal cord vibration, carotid pulse, radial pulse, elbow movement, fingers bend, and knee movement, have been monitored to demonstrate its biomedical detection capability as a wearable device.

Speech is an important tool for human communication, among which voice is the foundation of speech, and the vibration of vocal cords is the key to the production of voice. The abnormal voice caused by irregular vibration due to various causes is an acoustic signal reflecting the pathological changes of the larynx.[80] The recorded signals when the tester is speaking different words, such as "hello, sensor, biodegradable" are exhibited in **Figure 4**a. The results show different vocal cord vibrations can be recognized by attaching this pressure sensor onto surface of throat since every different word has its own characteristic peaks, manifesting the capability of voice recognition.

In addition, heart rate or pulse, as one of the most vital signs of the human body, has crucial denotative meaning for physical health of human. Thus, the repeatable carotid and radial pulse signals have been recorded in real time with regular shapes within 6 s based on the leaf vein-based pressure sensors, as displayed in Figure 4b,e. Three characteristic peaks, namely P (percussion wave), T (tidal wave), and D (diastolic wave) can be precisely received, which indicating high sensitivity of the device, and the experimenter's pulse rate of approximately 89 beats min$^{-1}$ can be correspondingly reckoned.

Our leaf vein-based pressure sensor not only shows a good response to tiny vibration monitoring, but also can be used to track the bending motion of human joints. Then, the devices are attached to the elbow, finger, and knee joints, respectively, to record the movement of bending-release cycle. Among them, the bending angle of elbow is 30°, 60°, 90°, 120°, and 150°; the bending angle of finger is 30°, 60°, 90°, and 120°; as well as the knee joint is 10°, 45°, 90°, and 135°. As shown in Figure 4c,d,f, similarly, the current signals present a good real-time response and repeatability under a certain joint bending angle, indicating that our leaf vein-based pressure sensor has good reliability and working stability in practical application. With the increase of bending angle, the variation magnitude of the current is significantly enhanced, and every bending angle can be distinctly observed. The slight difference at the same bending angle may be caused by the inconsistent movement behavior of the experimenter. The results show that the pressure sensor based on leaf vein can distinguish the motion angle of human joints in real time, providing great potential in biomedical and rehabilitated applications.

Additionally, tiny detection of airflow can also be realized based on the leaf vein-based pressure sensors, with results shown in **Figure 5**a. An instantaneous, stable, and repeatable response to a small airflow can be observed, laying a foundation for the potential application in micro air flowmeter. In order to prove the feasibility of our leaf vein-based pressure sensors in multipoint pressure identification, a 3 × 3 array has been fabricated, with optical photos illustrated in Figure 5b. Each pixel of the array can independently identify the position and magnitude of the external applied pressure when a weight is placed in the center of the array. Furthermore, a 1 × 7 pressure sensor array is integrated for wearable flexible electronic piano keyboard, covering seven musical scale from Do to Si (Figure 5c i–iii). Real-time resistance signal array is collected through the multichannel signal acquisition system, and then connected to the real-time display system via the wireless Bluetooth module. The prepared leaf vein-based piano keyboard can be bent, twisted, and worn, indicating the excellent flexibility of it. Under external pressure, the corresponding pixel responds to the press in real time, producing a corresponding frequency to each note, and a song is successfully played with it (seen in Movie S1, Supporting Information).

## 3. Conclusion

We have successfully developed a wearable piezoresistive multilayer pressure sensor based on natural leaf veins and NF films for real-time monitoring of human physiological signals and human-machine interface applications. Natural leaf vein/Ag NWs, as the pressure sensing layer, its inherent
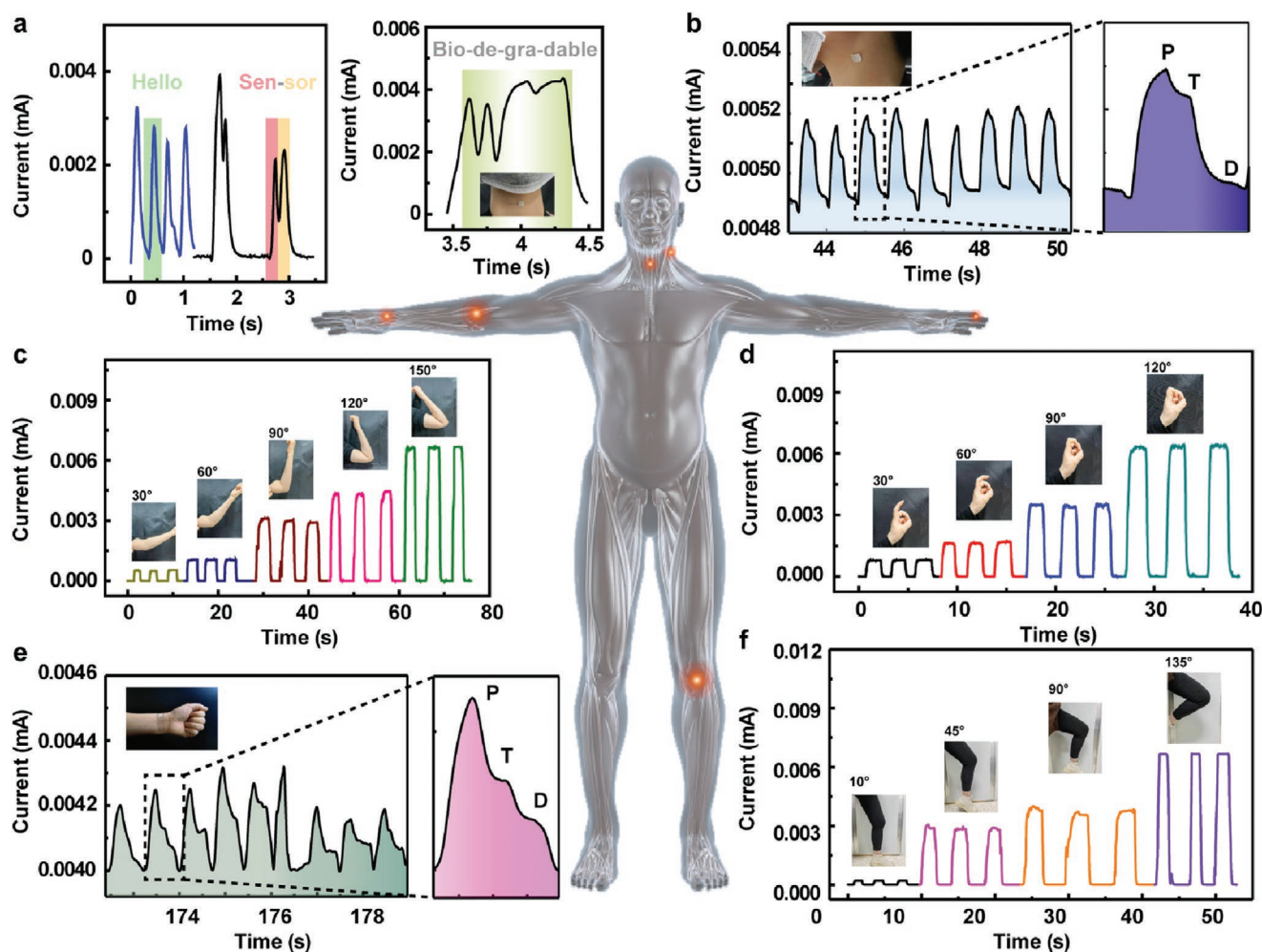
**Figure 4.** The monitoring and detection of human physiological signal and joint movement. a) Voice recognition achieved by monitoring the vibration of vocal cords. b) Pulse monitoring of the carotid artery. Local magnification on the right shows three characteristic peaks of typical pulse wave, namely P (percussion wave), T (tidal wave), and D (diastolic wave). c) Detection of the elbow joint movement. The motion angles of elbow joint are 30°, 60°, 90°, 120°, and 150°, respectively. d) Detection of the bending movement of the index finger. The motion angles of finger are 30°, 60°, 90°, and 120°, respectively. e) Pulse monitoring of the radial artery. Local magnification on the right shows three characteristic peaks of typical pulse wave, namely P (percussion wave), T (tidal wave) and D (diastolic wave). f) Detection of the knee joint movement. The motion angles of knee joint are 10°, 45°, 90°, and 135°.

fractal structure maximizes the specific surface area, which is beneficial to the improvement of the electrical output performance. The sensitivity of the leaf vein-based pressure sensor reaches 6.33 kPa$^{-1}$ within the linear sensing range of 0.03 to 11.6 kPa, and the device can still work stably after 6000 loading-unloading cycles. Through COMSOL simulation and theoretical analysis, the effect of multilayer structure on the electrical output performance of the device is further debated, and a strategy that can be used to modulate the device performance by the number of layers of active layers is proposed. Notably, the materials of whole devices are biodegradable, breathable, and good biocompatible. By combining with the electrospinning technology, PLGA and PVA NF films are prepared, which are integrated with natural leaf veins to produce devices with excellent air permeability. The hindrance to the evaporation of water vapor molecules at room temperature is very small and almost negligible. Besides, after 45 days of degradation tests in vitro, the weight loss of the whole device is about 50%. Finally, we localize it in the human body to monitor major physiological signals and motor behavior. As well as, a single device is further integrated into a $3 \times 3$ array for pressure imaging to achieve multipoint detection. Furthermore, a $1 \times 7$ sensor array is combined with the multichannel signal acquisition system and real-time display to develop a wearable flexible electronic piano keyboard. The pressure sensor based on leaf veins has prominent advantages in environmental friendliness, and electrical output performance can meet the current needs. There is no doubt that our research further promotes the development of wearable devices in practical aspects such as comfort, environmental friendliness, high mechanical stability, high sensitivity, and wide detection range. Looking for a new environmental friendly material is also one of the directions of our future efforts, and the sensor has room for further optimization and improvement.
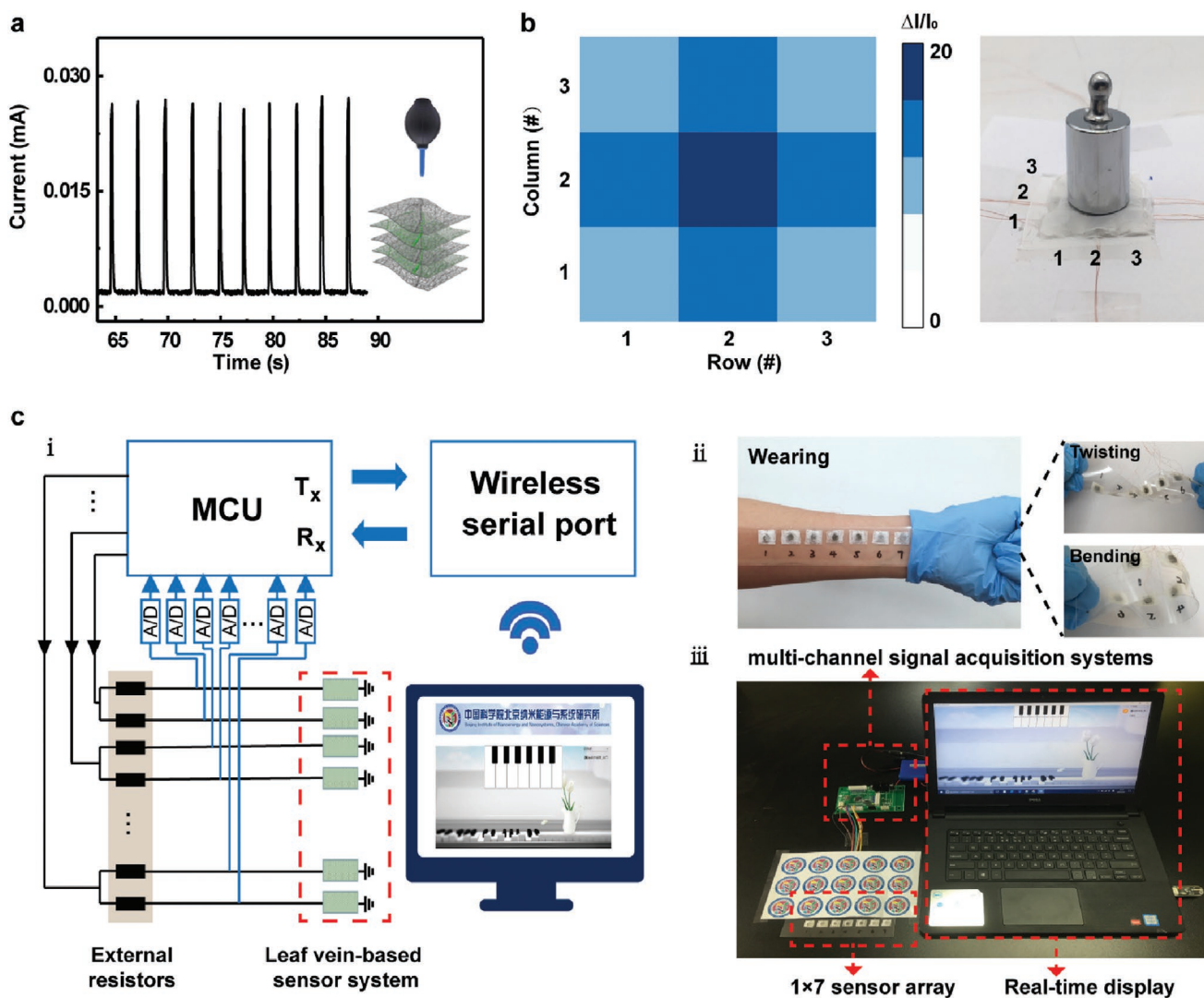
**Figure 5.** Detection capability of single point/multipoint of the leaf vein-based pressure sensor and integration of the piano keyboard system. a) Single point detection of the device. The device shows an instantaneous and stable response to a weak air flow. b) Multipoint of a 3 × 3 array detection of the device mapping. Pressure mapping profile (left) and optical photograph (right) illustrate the pressure distribution and amplitude of each pixel when the weight (50 g) placed on the array. c) Integration of the piano keyboard system. i. Schematic diagram of multichannel signal acquisition systems. Data acquisition, processing, and real-time display are accomplished by wireless connection to computer through home-made design; ii. Photographs of the flexibility of piano keyboard (wearing, twisting, bending); iii. Photograph of the flexible piano keyboard.

## 4. Experimental Section

*Fabrication of the Leaf Vein-Based Pressure Sensor*: (i) Some clear, tough magnolia leaves were soaked into the boiled NaOH solution with concentration of 35 wt%. Stirred the solution to separate the leaves and heat evenly, and kept heating the breaker for 6–8 min. When the leaf was corroded, the soft parts were easily removed with the veins left. Then, the remnant soft parts of the leaves were removed away by a soft brush under the running water. Finally, the complete leaf veins would be cleaned by the distilled water and dried in the air for 3 h.

(ii) PVA precursor solution with concentration of 9–11 wt% was prepared by dissolving PVA in deionized water and stirred about 2 h at 90°C. The PVA solution was injected into a plastic syringe with a 20-size electrospinning needle, and a board covered with aluminum foil acted as a collector. Then the PVA NF film was obtained by electrospinning with the following conditions: high voltage of 25 kV, a constant flow rate of 0.5 mL h$^{-1}$, and the working distance of 15 cm. After electrospinning,

the PVA NF film was dried at room temperature to remove residual moisture, and then carefully stripped from the aluminum foil.

(iii) Ag NWs with the diameter and the length of 150 nm with and 50 μm, were transferred onto PVA NF and leaf vein by spraying method, receiving PVA/Ag NWs NF films and leaf vein/Ag NWs. Then, flexible Au electrodes were attached to the surface as the lead-out electrodes.

(iv) PLGA was dissolved in HFIP with a solution concentration of 6.5–9.5 wt% as the precursor and then stirred for 12 h. The PLGA solution was injected into a plastic syringe containing a 23-size electrospinning needle. Then, PLGA NF film was prepared by electrospinning with the following conditions: high voltage of 15 kV, a constant flow rate of 0.45 mL h$^{-1}$, and the working distance of 15 cm. The PLGA NF film was dried in a vacuum drying oven at room temperature for 24 h.

(v) In order to fabricate the multilayer device, leaf vein and leaf vein/ Ag NWs were alternately stacked between top and bottom, PVA/Ag NWs NF film electrodes. And the device was encapsulated with PLGA NF films.

**ADVANCED
SCIENCE NEWS**

www.advancedsciencenews.com

**NANO · MICRO
small**

www.small-journal.com

*In Vitro Biodegradation Test*: Five NF films were tested for biodegradability in vitro, which were PVA, PLGA, PVA/Vein/PVA, PLGA/Vein/PLGA, and the whole device (PLGA/PVA/Vein/PVA/PLGA). Five NF films were separately placed in five 100-mL centrifuge tubes. Then, 50-mL sterilized PBS solution (pH≈7.4) was poured into each centrifuge tube for the biodegradation test. Then, the five centrifuge tubes containing different films were placed in an incubator at 37°. After each 15 days, the degradation of each NF film was recorded and the PBS solution was replaced with a new one. Finally, the nanofiber films in every PBS solution were taken out and washed with deionized water for five times, dried at 70 °C overnight, and weighed. The weight loss ratio was calculated by a simple formula: weight loss (wt%) = $(W_0 - W_n)/W_0 \times 100$, where $W_0$ was the initial weight and $W_n$ was the weight at a given degradation day.

*Characterizations and Measurements of the Leaf Vein-Based Pressure Sensor*: The surface morphologies of leaf veins and NF films were measured by scanning electron microscopy (SU1510 Hitachi). The thickness and surface roughness of leaf vein were measured by a surface profiler (KLA-Tencor P7). The contact angle of the NF films was characterized by the contact angle analyzer (XG-CAMB1). The chemical composition and structural characteristics of NF films were characterized by Fourier transform infrared spectrometer (VERTEX80v, Brucker). External pressure applied to the device controlled by a linear motor (Linmot E1100) was recorded by a dynamometer (Nano17, ATI). The electrical output performances were recorded with the Stanford Research System (SR 570 low noise current amplifier equipped with DS 345 synthesized function generator) under a sampling rate of 10 kHz.

*Leaf Vein-Based Piano Keyboard Demonstration*: The leaf vein-based sensor system consisted of seven separate unit sensors integrated on a PET film. Multichannel signal acquisition system was based on PIC16F1526 MCU. The signal acquisition system could collect data of 30 resistive sensors at the same time, and 20 groups of data per second had been recorded. The signal acquisition system and PC were connected through wireless serial port. The piano playing program written by C language can read the system data and complete the corresponding instructions.

In the test, a commercial nitrile glove was used to separate the volunteer's skin from the SMTE, which has no physical or psychological effect on the human body. After the experiments, no physical or psychological effect on the volunteer was observed. The volunteers in this study provided written informed consent.

## Supporting Information

Supporting Information is available from the Wiley Online Library or from the author.

## Conflict of Interest

The authors declare no conflict of interest.

## Data Availability Statement

The data that support the findings of this study are available from the corresponding author upon reasonable request.

[1] F. L. Gurgoglione, G. Niccoli, *Int. J. Cardiol.* **2021**, *328*, 197.
[2] Y. Lu, X. Y. Qu, W. Zhao, Y. F. Ren, W. L. Si, W. J. Wang, Q. Wang, W. Huang, X. C. Dong, *Research* **2020**, *11*, 2038560.
[3] G. Ge, Y. Lu, X. Y. Qu, W. Zhao, Y. F. Ren, W. J. Wang, Q. Wang, W. Huang, X. C. Dong, *ACS Nano* **2020**, *14*, 218.
[4] F. T. Li, J. F. Lu, Q. L. Zhang, D. F. Peng, Z. Yang, Q. Xu, C. F. Pan, A. L. Pan, T. F. Li, R. M. Wang, *Sci. Bull.* **2019**, *64*, 698.
[5] J. H. Liu, Z. C. Zhang, S. Qiao, G. S. Fu, S. F. Wang, C. F. Pan, *Sci. Bull.* **2020**, *65*, 477.
[6] Q. L. Hua, J. L. Sun, H. T. Liu, R. R. Bao, R. M. Yu, J. Y. Zhai, C. F. Pan, Z. L. Wang, *Nat. Commun.* **2018**, *9*, 244.
[7] B. S. Wan, S. Q. Guo, J. C. Sun, Y. F. Zhang, Y. Y. Wang, C. F. Pan, J. Y. Zhang, *Sci. Bull.* **2019**, *64*, 254.
[8] J. Tao, M. Dong, L. Li, C. F. Wang, J. Li, Y. Liu, R. R. Bao, C. F. Pan, *Microsyst. Nanoeng.* **2020**, *6*, 62.
[9] R. Ghosh, M. Song, J. Park, Y. Tchoe, P. Guha, W. Lee, Y. Lim, B. Kim, S. Kim, M. Kim, G. Yi, *Nano Energy* **2021**, *80*, 105537.
[10] R. R. Bao, C. F. Pan, *Sci. Bull.* **2020**, *65*, 1228.
[11] K. K. Zhou, Y. Zhao, X. P. Sun, Z. Q. Yuan, G. Q. Zheng, K. Dai, L. W. Mi, C. F. Pan, C. T. Liu, C. Y. Shen, *Nano Energy* **2020**, *70*, 104546.
[12] G. Ge, W. Yuan, W. Zhao, Y. Lu, Y. Z. Zhang, W. J. Wang, P. Chen, W. Huang, W. L. Si, X. C. Dong, *J. Mater. Chem. A* **2019**, *7*, 5949.
[13] C. F. Wang, C. F. Pan, Z. L. Wang, *ACS Nano* **2019**, *13*, 12287.
[14] W. K. Lin, B. Wang, G. X. Peng, Y. Shan, H. Hu, Z. B. Yang, *Adv. Sci.* **2021**, *8*, 2002817.
[15] Y. Liu, R. R. Bao, J. Tao, J. Li, M. Dong, C. F. Pan, *Sci. Bull.* **2020**, *65*, 70.
[16] K. L. Xia, W. Q. Wu, M. J. Zhu, X. Y. Shen, Z. Yin, H. M. Wang, S. Li, M. C. Zhang, H. M. Wang, H. J. Lu, A. L. Pan, C. F. Pan, Y. Y. Zhang, *Sci. Bull.* **2020**, *65*, 343.
[17] C. F. Pan, L. Dong, G. Zhu, S. M. Niu, R. M. Yu, Q. Yang, Y. Liu, Z. L. Wang, *Nat. Photonics* **2013**, *7*, 752.
[18] C. F. Pan, J. Y. Zhai, Z. L. Wang, *Chem. Rev.* **2019**, *119*, 9303.
[19] S. Huang, Y. L. Huang, Q. Li, *Small Struct.* **2021**, *2*, 2100038.
[20] Y. N. Ma, Y. Yue, H. Zhang, F. Cheng, W. Q. Zhao, J. Y. Rao, S. J. Luo, J. Wang, X. L. Jiang, Z. T. Liu, N. S. Liu, Y. H. Gao, *ACS Nano* **2018**, *12*, 3209.
[21] X. Y. Cao, J. Zhang, S. W. Chen, R. J. Varley, K. Pan, *Adv. Funct. Mater.* **2020**, *30*, 2003618.
[22] M. Zhu, Y. Yue, Y. F. Cheng, Y. N. Zhang, J. Su, F. Long, X. L. Jiang, Y. N. Ma, Y. H. Gao, *Adv. Electron. Mater.* **2020**, *6*, 1901064.
[23] K. B. Franke, H. Marshall, P. Kennewell, H.-D. Pham, P. J. Tully, T. Rattanakosit, G. Mahadevan, R. Mahajan, *Int. J. Cardiol.* **2021**, *328*, 130.
[24] H. C. Yao, T. Sun, J. S. Chiam, M. Tan, K. Y. Ho, Z. J. Liu, B. C. K. Tee, *Adv. Funct. Mater.* **2021**, *31*, 2008650.
[25] H. Liu, X. Y. Chen, Y. J. Zheng, D. B. Zhang, Y. Zhao, C. F. Wang, C. F. Pan, C. T. Liu, C. Y. Shen, *Adv. Funct. Mater.* **2021**, *31*, 2008006.
[26] D. F. Peng, X. H. Liu, C. F. Pan, *Sci. Bull.* **2020**, *66*, 6.
[27] H. Liu, Q. M. Li, Y. B. Bu, N. Zhang, C. F. Wang, C. F. Pan, L. W. Mi, Z. H. Guo, C. T. Liu, C. Y. Shen, *Nano Energy* **2019**, *66*, 104143.
[28] W. Feng, D. Q. Liu, D. J. Broer, *Small Struct.* **2020**, *2*, 2000107.
[29] G. B. Jia, J. Plentz, A. Dellith, C. Schmidt, J. Dellith, G. Schmidl, G. Andra, *Nano-Micro Lett.* **2020**, *12*, 19.

[30] Y. Lee, J. Park, S. Cho, Y.-E. Shin, H. Lee, J. Kim, J. Myoung, S. Cho, S. Kang, C. Baig, H. Ko, *ACS Nano* **2018**, *12*, 4045.

[31] J. Li, R. R. Bao, J. Tao, Y. Y. Peng, C. F. Pan, *J. Mater. Chem. C* **2018**, *6*, 11878.

[32] Y. Y. Peng, J. F. Lu, D. F. Peng, W. D. Ma, F. T. Li, Q. S. Chen, X. D. Wang, J. L. Sun, H. T. Liu, C. F. Pan, *Adv. Funct. Mater.* **2019**, *29*, 1905051.

[33] J. L. Sun, N. X. Li, L. Dong, X. X. Niu, M. Q. Zhao, Z. Q. Xu, H. P. Zhou, C. X. Shan, C. F. Pan, *Nanotechnology* **2021**, *32*, 475204.

[34] C. Z. Liao, F. Antaw, A. Wuethrich, W. Anderson, M. Trau, *Small Struct.* **2020**, *1*, 2000011.

[35] S. Gong, W. Schwalb, Y. W. Wang, Y. Chen, Y. Tang, J. Si, B. Shirinzadeh, W. L. Cheng, *Nat. Commun.* **2014**, *5*, 3132.

[36] N. Q. Luo, W. X. Dai, C. L. Li, Z. Q. Zhou, L. Y. Lu, C. C. Y. Poon, S. C. Chen, Y. T. Zhang, N. Zhao, *Adv. Funct. Mater.* **2016**, *26*, 1178.

[37] Y. Y. Qin, Q. Y. Peng, Y. J. Ding, Z. S. Lin, C. H. Wang, Y. Li, F. Xu, J. J. Li, Y.e. Y. X. D. He, Y. B. Li, *ACS Nano* **2015**, *9*, 8933.

[38] Y. Si, X. Q. Wang, C. C. Yan, L. Yang, J. Y. Yu, B. Ding, *Adv. Mater.* **2016**, *28*, 9512.

[39] C.-L. Choong, M.-B. Shim, B.-S. Lee, S. Jeon, D.-S. Ko, T.-H. Kang, J. Bae, S. H. Lee, K.-E. Byun, J. Im, Y. J. Jeong, C. E. Park, J.-J. Park, U.-I. Chung, *Adv. Mater.* **2014**, *26*, 3451.

[40] M. X. Xu, F. Li, Z. Y. Zhang, T. Shen, J. J. Qi, *Adv. Electron. Mater.* **2019**, *5*, 1800461.

[41] J. Y. Huang, D. W. Li, M. Zhao, H. Z. Ke, A. Mensah, P. F. Lv, X. J. Tian, Q. F. Wei, *Chem. Eng. J.* **2019**, *373*, 1357.

[42] C. H. Mu, Y. Q. Song, W. T. Huang, A. Ran, R. J. Sun, W. H. Xie, H. W. Zhang, *Adv. Funct. Mater.* **2018**, *28*, 1707503.

[43] X.-P. Li, Y. Li, X. F. Li, D. K. Song, P. Min, C. Hu, H.-B. Zhang, N. Koratkar, Z.-Z. Yu, *J. Colloid Interface Sci.* **2019**, *542*, 54.

[44] M. Worku, A. Ben-Akacha, T. B. Shonde, H. Liu, B. Ma, *Small Sci.* **2021**, *1*, 2000072.

[45] Y. Y. Shen, C. Z. Yan, K. B. Lin, Y. P. Zhao, S. R. Xu, B. Zhou, Z. H. Wei, K. Y. Yan, *Small Sci.* **2021**, *1*, 2000077.

[46] X.-Y. Qian, Y.-Y. Tang, W. Zhou, Y. Shen, M.-L. Guo, Y.-Q. Li, J.-X. Tang, *Small Sci.* **2021**, *1*, 2000048.

[47] Y. T. Zou, L. Cai, T. Song, B. Q. Sun, *Small Sci.* **2021**, *1*, 2000050.

[48] C.-K. Liu, H.-L. Loi, J. P. Cao, G. Q. Tang, F. Liu, Q. Huang, X. L. Liang, F. Yan, *Small Struct.* **2021**, *2*, 2000084.

[49] S. Pyo, J. Lee, W. Kim, E. Jo, J. Kim, *Adv. Funct. Mater.* **2019**, *29*, 1902484.

[50] X. R. Hu, T. Huang, Z. D. Liu, G. Wang, D. Chen, Q. L. Guo, S. W. Yang, Z. W. Jin, J.-M. Lee, G. Q. Ding, *J. Mater. Chem. A* **2020**, *8*, 14787.

[51] W. Q. Wu, X. D. Wang, X. Han, Z. Yang, G. Y. Gao, Y. F. Zhang, J. F. Hu, Y. W. Tan, A. L. Pan, C. F. Pan, *Adv. Mater.* **2019**, *31*, 1805913.

[52] F. Li, Z. G. Xia, C. F. Pan, Y. Gong, L. Gu, Q. L. Liu, J. Z. Zhang, *ACS Appl. Mater. Interfaces* **2018**, *10*, 11739.

[53] Z. Lou, G. Z. Shen, *Small Struct.* **2021**, *2*, 2000152.

[54] J. G. Bastidas, N. Maurmann, M. R. da Silveira, C. A. Ferreira, P. Pranke, *Biomed. Mater.* **2020**, *15*, 055014.

[55] M.-J. Lu, F.-Z. Chen, J. Hu, H. Zhou, G. X. Chen, X.-D. Yu, R. Ban, P. Lin, W.-W. Zhao, *Small Struct.* **2021**, *2*, 2100087.

[56] X. Zhang, W. F. Liu, D. T. Sun, J. H. Huang, X. Q. Qiu, Z. X. Li, X. X. Wu, *ChemSusChem* **2020**, *13*, 4774.

[57] X. Peng, K. Dong, C. Y. Ye, Y. Jiang, S. Y. Zhai, R. W. Cheng, D. Liu, X. P. Gao, J. Wang, Z. L. Wang, *Sci. Adv.* **2020**, *6*, eaba9624.

[58] T. A. Comerford, E. Zysman-Colman, *Small Sci.* **2021**, 2100022.

[59] S. Park, Y.-H. Kim, S. Kang, D. Lim, J. Park, D. Jang, S. Choi, J. Kim, S. Han, T.-W. Lee, S. Park, *Small Sci.* **2021**, *1*, 2000042.

[60] Y. Jiang, K. Dong, J. An, F. Liang, J. Yi, X. Peng, C. Ning, C. Ye, Z. L. Wang, *ACS Appl. Mater. Interfaces* **2021**, *13*, 11205.

[61] W. L. Lu, R. Hu, X. Tong, D. P. Yu, Q. Zhao, *Small Struct.* **2020**, *1*, 2000003.

[62] V. Sharma, A. Koivikko, K. Yiannacou, K. Lahtonen, V. Sariola, *npj Flexible Electron.* **2020**, *4*, 27.

[63] H. L. Zhang, D. F. Peng, W. Wang, L. Dong, C. F. Pan, *J. Phys. Chem. C* **2015**, *119*, 28136.

[64] X. Y. Li, M. X. Chen, R. M. Yu, T. P. Zhang, D. S. Song, R. R. Liang, Q. L. Zhang, S. B. Cheng, L. Dong, A. L. Pan, Z. L. Wang, J. Zhu, C. F. Pan, *Adv. Mater.* **2015**, *27*, 4447.

[65] S. Qiao, R. D. Cong, J. H. Liu, B. L. Liang, G. S. Fu, W. Yu, K. L. Ren, S. F. Wang, C. F. Pan, *J. Mater. Chem. C* **2018**, *6*, 3233.

[66] Y. N. Sun, T. Liu, Y. Y. Kan, K. Gao, B. Tang, Y. L. Li, *Small Sci.* **2021**, *1*, 2100001.

[67] X. Jiang, K. Wang, H. Wang, L. J. Duan, M. Y. Du, L. K. Wang, Y. X. Cao, L. Liu, S. P. Pang, S. Z. Liu, *Small Sci.* **2021**, *1*, 2000054.

[68] K. Ma, S.-N. Hsu, Y. Gao, Z. T. Wei, L. R. Jin, B. P. Finkenauer, L. B. Huang, B. W. Boudouris, J. G. Mei, L. T. Dou, *Small Sci.* **2021**, *1*, 2000024.

[69] H. Zhang, G. P. Chen, Y. R. Yu, J. H. Guo, Q. Tan, Y. J. Zhao, *Adv. Sci.* **2020**, *7*, 2070090.

[70] C. Perezcampos Mayoral, J. Gutierrez Gutierrez, J. L. Cano Perez, M. Vargas Trevino, I. B. Gallegos Velasco, P. A. Hernandez Cruz, R. Torres Rosas, L. Tepech Carrillo, J. Arnaud Rios, E. L. Apreza, R. Rojas Laguna, *Biosensors* **2021**, *11*, 58.

[71] M. Nishinaka, H. Jinno, Y. Jimbo, S. Lee, J. Wang, W. Lee, T. Yokota, T. Someya, *Small Struct.* **2020**, *2*, 2000088.

[72] J. Li, R. R. Bao, J. Tao, M. Dong, Y. F. Zhang, S. Fu, D. F. Peng, C. F. Pan, *Appl. Phys. Rev.* **2020**, *7*, 011404.

[73] U. P. Claver, G. Zhao, *Adv. Eng. Mater.* **2021**, *23*, 2001187.

[74] A. Mazzanti, E. A. A. Pogna, L. Ghirardini, M. Celebrano, A. Schirato, G. Marino, A. Lemaître, M. Finazzi, C. D. Angelis, G. Leo, G. Cerullo, G. D. Valle, *Small Sci.* **2021**, *1*, 2000079.

[75] J. He, Y. F. Zhang, R. H. Zhou, L. R. Meng, T. Chen, W. J. Mai, C. F. Pan, *J. Materiomics* **2020**, *6*, 86.

[76] Z. W. Wang, J. Chen, Y. Cong, H. Zhang, T. Xu, L. Nie, J. Fu, *Chem. Mater.* **2018**, *30*, 8062.

[77] S. R. A. Ruth, V. R. Feig, M.-g. Kim, Y. Khan, J. K. Phong, Z. N. Bao, *Small Struct.* **2020**, *2*, 2000079.

[78] H. Ouyang, J. J. Tian, G. L. Sun, Y. Zou, Z. Liu, H. Li, L. M. Zhao, B. J. Shi, Y. B. Fan, Y. F. Fan, Z. L. Wang, Z. Li, *Adv. Mater.* **2017**, *29*, 1703456.

[79] K. K. Zhou, K. Dai, C. T. Liu, C. Y. Shen, *SmartMat* **2020**, *1*, e1010.

[80] Z. C. Zhang, B. Zhao, D. Y. Shen, Q. Y. Tao, B. Li, R. X. Wu, B. L. Li, X. D. Yang, J. Li, R. Song, H. M. Zhang, Z. W. Huang, Z. W. Zhang, J. Y. Zhou, Y. Liu, X. D. Duan, *Small Struct.* **2021**, *2*, 2100028.